Digital notch filter based active damping for LCL filters

Yao, Wenli; Yang, Yongheng; Zhang, Xiaobin; Blaabjerg, Frede

Published in:
Proceedings of the 2015 IEEE Applied Power Electronics Conference and Exposition (APEC)

DOI (link to publication from Publisher):
10.1109/APEC.2015.7104684

Publication date:
2015

Document Version
Early version, also known as pre-print

Digital Notch Filter based Active Damping for *LCL* Filters

Wenli Yao[†],Yongheng Yang[‡], Xiaobin Zhang[†], Frede Blaabjerg[‡]

[†]School of Automation
Northwestern Polytechnical University
127 Youyi West Road, Xi'an, Shaanxi, 710072, P.R.China
mjkfhill@live.com, dgl907@126.com

[‡]Department of Energy Technology
Aalborg University
Pontoppidanstraede 101, Aalborg, DK-9220 Denmark
yoy@et.aau.dk, fbl@et.aau.dk

***Abstract* — *LCL* filters are widely used in Pulse Width Modulation (PWM) inverters. However, it also introduces a pair of unstable resonant poles that may challenge the controller stability. The passive damping is a convenient possibility to tackle the resonance problem at the cost of system overall efficiency. In contrast, the active damping does not require any dissipation elements, and thus has become of increasing interest. As a result, a vast of active damping solutions have been reported, among which multi-loop control systems and additional sensors are necessary, leading to increased cost and complexity. In this paper, a notch filter based active damping without the requirement of additional sensors is proposed, where the inverter current is employed as the feedback variable. Firstly, a design method of the notch filter for active damping is presented. The entire system stability has then been investigated, which has revealed that negative variations of the resonant frequency can seriously affect the system stability. In order to make the controller more robust against grid impedance variations, the notch filter frequency is thus designed smaller than the *LCL* filter resonant frequency, which is done in the *z*-domain. Simulations and experiments are carried out to verify the proposed active damping method. Both results have confirmed that the notch filter based active damping can ensure the entire system stability in the case of resonances with a good system performance.**

I. INTRODUCTION

Pulse Width Modulation (PWM) inverters incorporated with *LCL* filters are commonly used as grid-connected converters, since they can provide an adjustable power factor and low harmonic current injections. As a third-order system, the *LCL* filter provides significantly improved attenuation of the PWM switching harmonics with a reduced overall size and weight, when it is compared with the conventional filter of a single inductor [1], [2]. Unfortunately, the *LCL* filter also introduces unstable poles that give magnitude peaks at the corresponding resonant frequencies. Such resonances may make the entire system unstable, being an increasing challenge to the controller design and also in the power system [3]-[5].

Usually, there are two possibilities to "trap" the unstable poles into a stable region: a) the passive damping based on dissipation elements in series or in parallel with the inductor or the capacitor of the *LCL* filter and b) the active damping that is included in the control system. As for the passive damping, additional losses hinder its applications in high power PWM converters. By contrast, the active damping aims at modifying the control algorithm so as to increase the stability margin at its resonance frequency. Many active damping solutions have been proposed in the literature. For example, a concept of the virtual resistor is introduced in [6], where an additional control loop by feeding back the capacitor current or voltage makes the filter behave like a "real" passive damping resistor. However, this method using a differentiator that may amplify high frequency noise. Nevertheless, a lead-lag network or an Infinity Impulse Response (IIR) digital filter that behaves as a differentiator can be adopted in the case of a virtual resistor based active damping [7]-[9]. Moreover, a new control strategy by feeding back the weighted average value of currents flowing through the split filtering capacitors to the current controller is proposed in [10], and in [11] the feedback term is instead the grid or the inverter current. These active damping approaches can be categorized as the multi-loop control systems, and thus additional sensors are required. In order to reduce the sensor requirement, the virtual flux is developed to estimate the capacitor voltage or the capacitor current [12]. Additionally, inserting a low-pass filter or a notch filter into the forward path of the current control loop can also achieve an active damping.

Initially, the notch concept was implemented in [13] by cascading a notch filter with the main controller, and thus the resonance of the *LCL* filter is dampened. Genetic algorithms are normally adopted in the notch filter, as it is presented in [14], where the tuning procedures and the limitations of different solutions are also discussed. However, the discretization of the notch filter is the main design challenge, since it will alter the pole and zero locations if designed inappropriately as discussed in [15]. As a consequence, the damping performance may be significantly degraded, and thus contributing to a possibility of resonating. In light of the above issues, a design method for the notch filter based active damping in the *z*-domain is presented first in this paper. In the proposed design solution, only two coefficients related to the bandwidth and the notch frequency respectively have to be determined [16], [17]. In addition, in order to make the controller more robust against grid impedance variations, the notch filter frequency is thus designed smaller than the *LCL* filter resonant frequency, which is done in the *z*-domain. Moreover, an analysis of the robustness against the *LCL* filter parameter and/or the grid impedance variations is carried out.

This paper is organized as follows. In § II, the system description is presented, where the control structure and the traditional notch filter based active damping method are

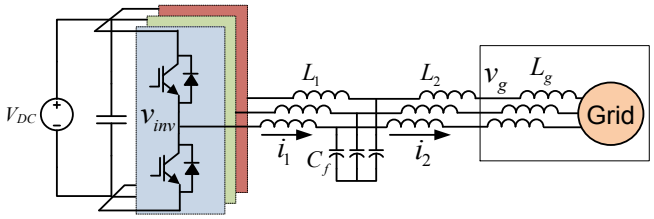

Fig. 1. Grid-connected inverter system with an *LCL*-filter.

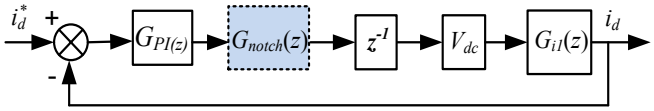

Fig. 2. Control structure of the closed-loop current control system with a notch filter based active damping, where i_d is the *d* axis current of i_1 in the *dq* frame.

TABLE I.
PARAMETERS OF THE THREE-PHASE GRID-CONNECTED PWM INVERTER WITH AN *LCL* FILTER.

Parameters	Symbol	Value
Power Rating	P_n	2.2 kW
Inverter Side Inductor	L_1	1.8 mH
Grid Side Inductor	L_2	2 mH
Filter Capacitor	C_f	4.7 uF
Resonant Frequency	f_{res}	2385 Hz
Grid Impedance	L_g	0~10 mH
Sampling Frequency	f_{sw}	10 kHz
Grid Voltage	V_g	230 V/50 Hz
DC Bus Voltage	V_{dc}	650 V

introduced. Then, the proposed design procedure of the notch filter based active damping method is developed in the *z*-domain in § III, where different discretization methods are compared with the proposed design method. In § IV, the sensitivity of the traditional notch filter based active damping is discussed in the case of varying resonant frequencies. In § V, the tuning procedure of the current controller with the proposed notch filter based active damping is described, as well as the robustness of the entire current controller is analyzed considering the *LCL* filter parameter and grid impedance variations. Simulation and experimental results are provided in § VI in order to verify the proposed notch filter based active damping method.

II. SYSTEM DESCRIPTION

Fig. 1 shows the structure of a grid-connected inverter with an *LCL* filter. In Fig. 1, L_1 and L_2 are the inverter side inductor and the grid side inductor, respectively, C_f is the filter capacitor, L_g is the grid inductor, and V_g the grid voltage. Subsequently, the transfer function of the *LCL* filter in the *z*-domain from the inverter output voltage V_1 to the inverter output current I_1 can be given as (1), where a Zero-Order-Hold (ZOH) is adopted for the discretization and the grid impedance is also taken into account.

$$G_{I1}(z)=\frac{i_1(z)}{v_{inv}(z)}=\frac{T_s}{(L_1+L_2+L_g)(z-1)}+\frac{(L_2+L_g)\sin\omega_{res}T_s}{\omega_{res}L_1(L_1+L_2+L_g)}\frac{(z-1)}{z^2-2z\cos\omega_{res}T_s+1} \quad (1)$$

$$\omega_{res}=\sqrt{\frac{L_1+L_2+L_g}{L_1\cdot(L_2+L_g)\cdot C_f}} \quad (2)$$

where $T_s = 1/f_s$ is the sampling period with f_s being the sampling frequency and ω_{res} is the resonant frequency of the *LCL* filter. It should be noted that the numerator of $G_{i1}(z)$ has an anti-resonant peak at the frequency of:

$$\omega_0=\sqrt{1/L_2C_f} \quad (3)$$

which leads to a less phase lag at the frequency below the resonant frequency.

The overall current control structure of the inverter is shown Fig. 2, in which a Proportional-Integral (PI) controller of (3) is adopted as the current controller. The proportional gain k_p of the PI controller can be tuned according to the optimized relationship between k_p and the crossover frequency ω_c by appointing a desired phase margin (e.g., PM = 60°); while, T_i can be calculated by ensuring that its phase contribution is small at the crossover frequency [18].

$$G_{PI}(s)=k_p\left(1+\frac{1}{T_i s}\right) \quad (4)$$

where the controller gains are designed as,

$$k_p=\frac{\omega_c(L_1+L_2)}{V_{dc}},\qquad T_i=\frac{10}{\omega_c}.$$

Considering the sampling, computation and PWM process, one-step pure delay z^{-1} is introduced in the current control system shown in Fig. 2. Besides, a notch filter is included in the control loop as the active damping to ensure the system stability. The transfer function of the notch filter can be given in the *s*-domain as,

$$G_{notch}(s)=\frac{s^2+\omega_n^2}{s^2+Qs+\omega_n^2} \quad (5)$$

in which Q is the quality factor of the notch filter determining the rejection bandwidth, ω_n is the notch frequency. In [13], [14], the rejection bandwidth ω_n is placed at the resonant frequency of the *LCL* filter ω_{res} in order to cancel out the resonant peaks induced by the *LCL* filter. Actually, this is a kind of zero-pole cancelling method. Notably, the notch filter based active damping is very sensitive to the resonant pole variations introduced by the unknown grid impedance changes, which will be discussed in details in § IV.

According to Fig. 2, the open-loop transfer function of the current control system can be expressed in the *z*-domain as,

$$G_{open}(z)=G_{PI}(z)\cdot G_{notch}(z)\cdot z^{-1}\cdot V_{dc}\cdot G_{i1}(z) \quad (6)$$

where V_{dc} is the DC-link voltage, and $G_{notch}(z)$ is the discretized transfer function of the notch filter given in (5). It should be noted that, when the converter current is employed as the feedback control variable, the current control system will be stable only in the case of very low resonant frequencies [13]. Table I shows the parameters of the PWM inverter with an *LCL* filter as shown in Fig. 1. Then, a basic analysis of the LCL filter resonance can be achieved. Fig. 3 shows the Bode plots of the *LCL* filter in (1), the notch filter in (5), and the open-loop control system in (6), where the notch filter based active damping is employed.

As it is shown in Fig. 3, the wide stable range is because the -180°-crossing happens only once, where the frequency lower

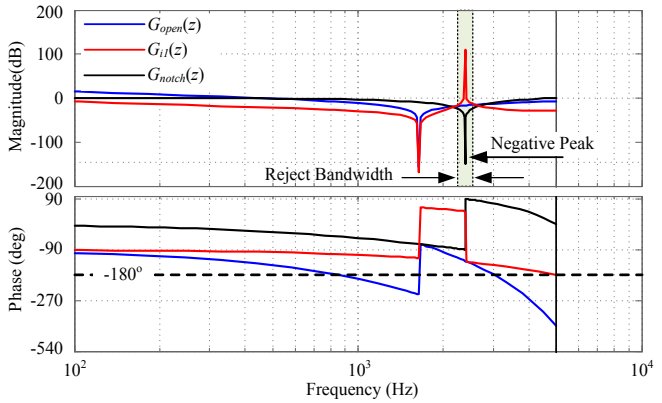

Fig. 3. Bode plot of the open-loop current controller with a traditional notch filter based active damping.

than the resonant frequency of the *LCL* filter where the gain is lower than 0 dB. However, for the higher resonance frequencies, there is one negative -180°-crossing with the gain above 0 dB. This indicates instability according to the Nyquist criteria. Hence, an effective damping is required for the *LCL* filter when the converter-current is feedback. The resonant peak of the *LCL* filter should be suppressed, and also the phase of the *LCL* filter should be compensated efficiently by introducing the notch filter. In that case, there will be no -180°-crossing with the gains above 0 dB. Consequently, the current control system stability is guaranteed.

III. Digital Notch Filter

As it is shown in Fig. 3, the notch filter has a narrow rejection bandwidth and an infinite negative gain around the notch frequency. In respect to the implementation of the notch filter in the digital form, the transfer function of (5) has to be discretized properly, since the notch frequency is sensitive to the discretization [15]. A slight error in the location of the notch frequency can contribute to a significant loss of the capability to suppress the *LCL* filter resonant peak. Actually, even for small notch frequency deviations, the effect on the active damping performance cannot be ignored. In general, there are two possibilities to design the notch filter. One can be done in the *s*-domain, and then a discretization method is applied to the *s*-domain model so as to implement it in the *z*-domain. Another option is directly to design the notch filter in the *z*-domain in order to reduce the phase and magnitude errors introduced by the discretization method, which will be done in the following.

A. Design of the Notch Filter in the z-Domain

In order to develop an accurate model of the digital notch filter by applying the Tustin transformation to the $G_{notch}(s)$, as following,

$$\begin{aligned} G_{notch}(z) &= G_{notch}(s)\Big|_{s=\frac{2}{T_s}\cdot\frac{z-1}{z+1}=k\cdot\frac{z-1}{z+1}} \\ &= \frac{\left(k^2+\omega_n^2\right)-2\left(k^2-\omega_n^2\right)z^{-1}+\left(k^2+\omega_n^2\right)z^{-2}}{\left(k^2+\omega_n^2+kQ\right)-2\left(k^2-\omega_n^2\right)z^{-1}+\left(k^2+\omega_n^2-kQ\right)z^{-2}} \end{aligned} \tag{7}$$

where the Tustin transformation can be given as,

$$s = k\cdot\frac{z-1}{z+1}. \tag{8}$$

If $k = \omega_n/\sin(\omega_n T_s/2)$, the discretization procedure of (7) is the so-called pre-warping Tustin method. In order to minimize the number of coefficients of the transfer function $G_{notch}(z)$, (7) is rewritten as,

$$G_{notch}(z) = \frac{1}{2}\cdot\frac{(1+a_2)-2a_1z^{-1}+(1+a_2)z^{-2}}{1-a_1z^{-1}+a_2z^{-2}} \tag{9}$$

in which,

$$\begin{cases} a_1 = \dfrac{2\left(k^2-\omega_n^2\right)}{k^2+\omega_n^2+kQ} \\ a_2 = \dfrac{k^2+\omega_n^2-kQ}{k^2+\omega_n^2+kQ} \end{cases} \tag{10}$$

It should be noted that the notch filter transfer function given by (9) is characterized by two parameters a_1 and a_2 as shown in (10). As a consequence, the notch filter $G_{notch}(z)$ can be conveniently implemented in a digital signal processor by including two multipliers of coefficients a_1 and a_2.

According to (7), the magnitude of the notch filter can be obtained as,

$$\left|G(e^{j\omega T_s})\right|^2 = \frac{\left\{\left(k^2+\omega_n^2\right)\cos\omega T_s-\left(k^2-\omega_n^2\right)\right\}^2}{\left\{\left(k^2+\omega_n^2\right)\cos\omega T_s-\left(k^2-\omega_n^2\right)\right\}^2+k^2Q^2\sin^2\omega T_s} \tag{11}$$

When the rejection bandwidth Ω and its minimum attenuation gain x of the notch filter are specified, the coefficients a_1 and a_2 can then be calculated as,

$$\begin{cases} a_1 = \dfrac{2\cos\omega_n T_s}{1+\lambda\cdot\tan\left(\Omega T_s/2\right)} \\ a_2 = \dfrac{1-\lambda\cdot\tan\left(\Omega T_s/2\right)}{1+\lambda\cdot\tan\left(\Omega T_s/2\right)} \end{cases} \tag{12}$$

where λ can be expressed by,

$$|\lambda| = \sqrt{10^{x/10}-1}. \tag{13}$$

It is indicated in (11) that the constants a_1 and a_2 are determined by the notch frequency ω_n and the desired rejection bandwidth Ω. Moreover, the quality factor Q is absent in (12). Actually, the quality factor Q is replaced by the following,

$$Q = \frac{1}{k\lambda}\left(k^2+\omega_n^2\right)\cdot\tan\left(\frac{\Omega T_s}{2}\right) \tag{14}$$

B. Comparison of Different Discretization Method Effects on the Digital Notch Filter

Different discretization methods have been deeply explored in [19] for the Proportional Resonant (PR) controller in terms of the discretization impact on the resonant pole displacement, the effect on zeros distribution, and the delay. It has been found that the Tustin transformation contributes to the most significant deviations. In contrast, other discretization methods, e.g., the ZOH method, the IMPulse invariant (IMP) method, the Pre-Warping Tustin (PWT) method, provide an accurate placement of the resonant peaks even at high resonant frequencies or with low sampling rates.

Actually, as it can be seen in (4), the transfer function of the notch filter $G_{notch}(s)$ is the reciprocal of a PR controller, where the proportional gain is one and the resonant gain is the quality factor Q. This PR controller can be given as,

TABLE II.
TRANSFER FUNCTIONS FOR THE PR CONTROLLER OF (14) USING DIFFERENT DISCRETIZATION METHODS.

Method	Transfer Function
Zero-Order-Hold	$G_{\mathrm{PR}-zoh}(z)=1+Q\cdot\frac{\sin(\omega_n T_s)}{\omega_n}\cdot\frac{z-1}{z^2-2\cdot\cos(\omega_n\cdot T_s)\cdot z+1}$
Pre-Warping Tustin	$G_{\mathrm{PR}-pwt}(z)=1+Q\cdot\frac{\sin(\omega_n T_s)}{2\omega_n}\cdot\frac{z^2-1}{z^2-2\cdot\cos(\omega_n\cdot T_s)\cdot z+1}$
IMPulse invariant	$G_{\mathrm{PR}-ipm}(z)=1+Q\cdot T_s\cdot\frac{z^2-\cos(\omega_n\cdot T_s)\cdot z}{z^2-2\cdot\cos(\omega_n\cdot T_s)\cdot z+1}$

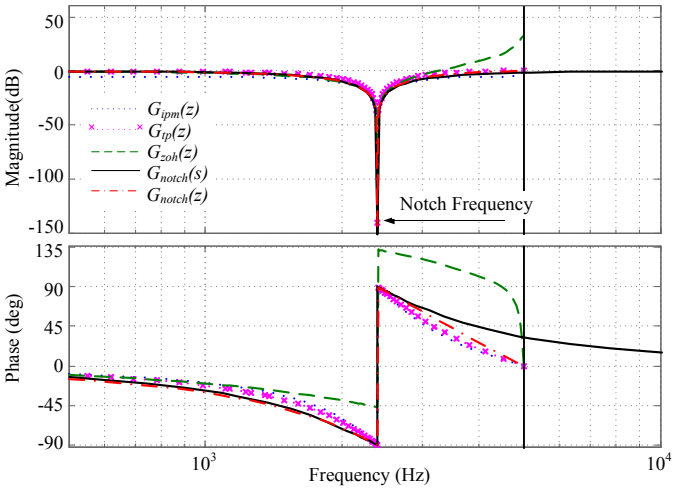

Fig. 4. Frequency responses of G_{notch}(s) and G_{notch}(z), where the sampling frequency f_s = 10 kHz.

$$G_{PR}(s)=\frac{1}{G_{notch}(s)}=1+\frac{Qs}{s^2+\omega_n^2} \tag{15}$$

which shows that the frequency response of the notch filter is symmetrical with 0 dB magnitude and zero phase lines. Applying the ZOH, IMP and PWT methods the PR controller $G_{PR}(s)$ of (15) results in the discretized expressions as shown in Table II, where the transfer functions are denoted as $G_{PR\text{-}zoh}(z)$, $G_{PR\text{-}ipm}(z)$ and $G_{PR\text{-}pwt}(z)$ correspondingly. Therefore, the discretized transfer functions of the notch filter using the aforementioned methods can be derived by simply inverting the numerator and the denominator of the corresponding transfer function shown in Table II, denote as $G_{zoh}(z)$, $G_{\text{-}ipm}(z)$ and $G_{pwt}(z)$ respectively.

As recommended in [13], considering the robustness, the reject bandwidth Ω is designed as $0.1\omega_{\mathrm{res}}$ and the maximum gain of rejection band is -20 dB. The quality factor of the notch filter Q can thus be calculated using (14). The notch frequency is selected at the resonant frequency of the *LCL* filter, which can be calculated form Table II as f_{res}=f_n=2385 Hz. Notably, the designed f_n is much higher than that in the PR controller as discussed in [19]. Fig. 4 compares the frequency responses of $G_{notch}(z)$, $G_{notch}(s)$ and its discretized transfer functions. As shown in Fig. 4, an almost equivalent magnitude behavior is observed around the notch frequency, although $G_{ipm}(z)$ has a lower gain in the whole frequency range. Moreover, Fig. 4 also confirms that $G_{zoh}(z)$ tends to increase the gain at high frequencies. It should be noted that $G_{tp}(z)$ tends to reduce the rejection bandwidth of the notch filter. As a result, this may make the notch filter based active damping more susceptible to a resonant frequency deviation. In general, the discretization will not contribute to much influence on the magnitude responses.

However, the phase frequency responses are significantly affected in those discretization methods. From Fig. 4, it can be observed that $G_{notch}(z)$ of (7) is the most accurate when comparing with the other discretization methods. On the contrary, the phase lags introduced by $G_{ipm}(z)$ and $G_{tp}(z)$ are lower than those of the continuous models. This is beneficial to increase the phase margin, although they also cause less phase leads in the region of higher frequencies, as it is shown in Fig. 4. Therefore, the implementation of the notch filter based on $G_{ipm}(z)$ and $G_{tp}(z)$ may result in insufficient capability to compensate the delays. Moreover, the ZOH produces a large phase lead after the notch frequency with a gain above 0 dB, which could affect the system stability. Fig. 4 also shows that $G_{notch}(z)$ of (7) can be considered the most advantageous implementation of $G_{notch}(s)$, since its magnitude and phase response are most close to $G_{notch}(s)$. Furthermore, $G_{notch}(z)$ provide larger phase lead than $G_{ipm}(z)$ and $G_{tp}(z)$ after the notch frequency.

IV. SENSITIVITY ANALYSIS OF THE TRADITIONAL NOTCH FILTER BASED ACTIVE DAMPING

A sensitivity analysis of the current control loop with the notch filter based active damping have been carried out in considering the *LCL* filter parameter variations, the grid impedance changes, and the computation delays. The nominal values of the grid-connected inverter system with an *LCL* filter has been shown in Table I, where the grid impedance variation range is also specified. Bode plots of both the open-loop and the closed-loop systems in the *z*-domain are employed to evaluate the system stability. The notch frequency is set to be the normal resonant frequency of the *LCL* filter, i.e., f_n = f_{res} = 2385 Hz.

It is indicated in (1) that a positive variation of the *LCL* filter parameters and the grid impedance will result in a negative change of the resonant frequency that may become below the notch frequency, vice versa. Fig. 5 further compares the open-loop Bode plots of the system with different resonant frequencies. As it can be seen in Fig. 5(a), the resonant frequency varies negatively from f_n to $0.92f_n$ when the grid side inductor is changed from 2 mH to 3 mH. As a result, the notch filter will lose the ability to suppress the resonant peak of the *LCL* filter. In the case of L_g = 2.8 mH, the phase of the notch filter is negative at the resonant frequency, which means that it is unable to compensate the phase of open loop not to cross -180°, leading to instability, as it is shown in Fig. 5(c). Nevertheless, when the resonant frequency varies positively from f_n to $1.22f_n$ by decreasing the grid side inductor from 2 mH to 1 mH, as it is shown in Fig. 5 (b), the phase of notch filter will be positive at the resonant frequency. This means that the notch filter is able to compensate the phase of the open-loop system not to cross -180° at the resonant frequency.

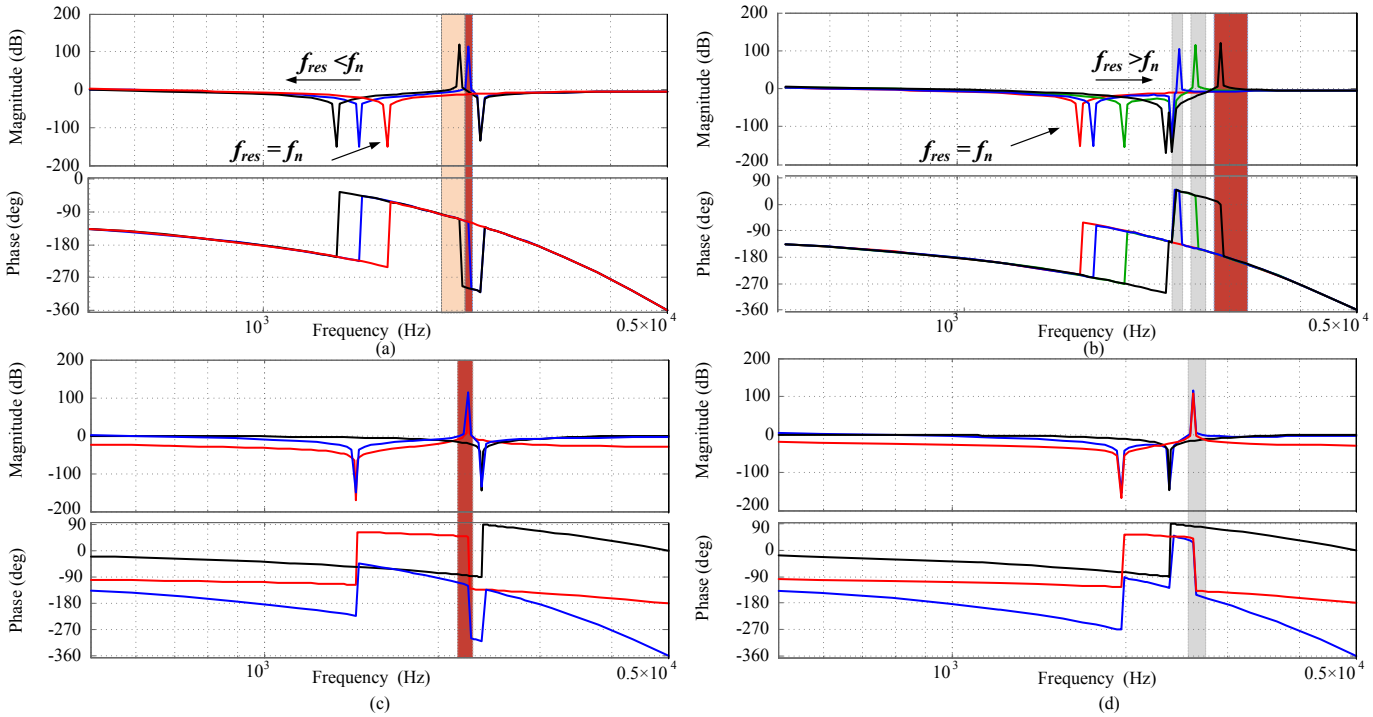

Fig. 5. Bode plot of open-loop with different resonant frequency: (a) $0.92f_n<f_{res}<f_n$, (b) $f_{res}=0.93f_n$, (c) $f_n<f_{res}<1.22f_n$, and (d) $f_{res}=1.1f_n$.

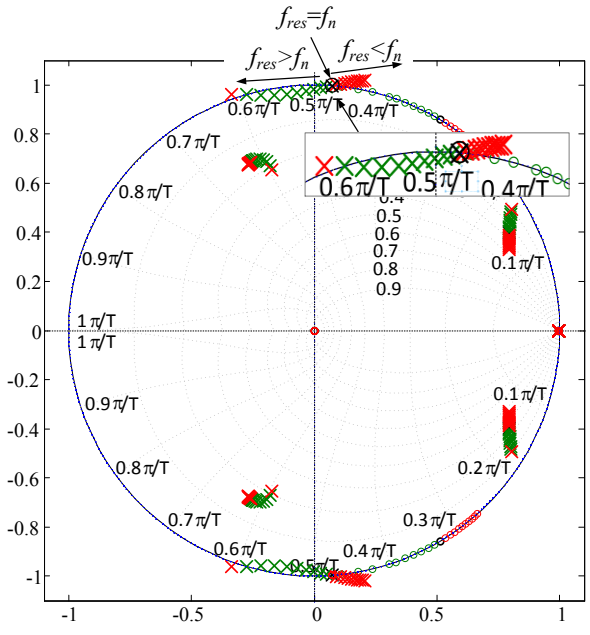

Fig. 6. Pole and zero maps of the closed-loop current control loop with different resonant frequencies ($0.92\,f_n<f_{res}<1.22\,f_{res}$).

Thus, the system is always stable even when the resonant peak of the *LCL* filter still exists. Additionally, in the case of a smaller grid impedance L_g = 1.4 mH, as it is shown in Fig. 5(d), the compensation of the phase lag is achieved. However, when the resonant frequency is too far from the notch frequency, the phase of the notch filter is insufficient to compensate the phase lag, as it is highlighted in Fig. 5(b). This can be further illustrated using the pole-and-zero plots of the closed-loop system, which can be given as,

$$G_{close}(z)=\frac{G_{PI}(z)\cdot G_{notch}(z)\cdot V_{dc}\cdot G_{i1}(z)}{z+G_{PI}(z)\cdot G_{notch}(z)\cdot V_{dc}\cdot G_{i1}(z)} \tag{16}$$

Then, the pole and zero maps of the closed-loop system with different resonant frequencies ($0.92f_n<f_{res}<1.22f_n$) can be obtained as Fig. 6. It can be seen in Fig. 6 that, when the resonant frequency is equal to the notch frequency, the unstable pole of the *LCL* filter is canceled out by the zero of the notch filter, and thus the system stability is secured. However, an increase of the resonant frequency will force the unstable pole away from the zeros of the notch filter and thus out of the unit cycle, thus challenging the entire system stability; whilst in the case of a negative resonant frequency change, the unstable poles will move into the unit cycle, resulting in a stable system. Nevertheless, if the resonant frequency decreases too much, the poles will go out of the unit circle, as shown in Fig. 6, and thus the entire system goes to be unstable.

One conclusion can be drawn from the above analysis is that the stability of the entire current control system is sensitive to the resonant frequency variations. In order to guarantee the closed-loop system stability, the notch frequency must be designed smaller than the resonant frequency of the *LCL* filter. This inspires to locate the notch frequency below the resonant frequency in order to increase the system stability margin. However, the PI controller and the notch filter should be designed carefully as demonstrated in the following.

V. Current Controller Design

The notch filter based active damping method should enhance the system stability. According to (9), only two parameter a_1 and a_2 associated with angular notch frequency

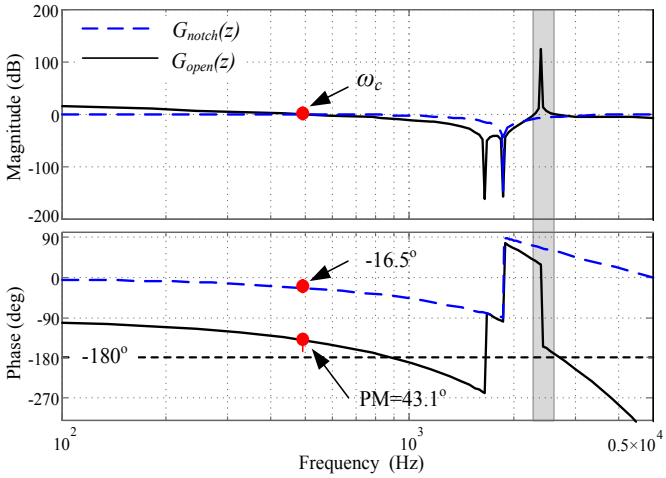

Fig. 7. Bode plot of the open-loop current control system when the notch frequency f_n is placed below the resonant frequency f_{res}.

ω_n and the stop bandwidth Ω have to be designed. Since the magnitude and phase contribution of the *LCL* filter resonance will become small at the crossover frequency, the *LCL* filter response will be dominated by the series inductance [3]. Besides, the PI controller also makes less phase contribution at the crossover frequency, i.e., $\angle G_{PI}(e^{j\omega cT}) \approx 0$. It is thus reasonable to approximate the *LCL*-filter as a single *L* filter ($L = L_1 + L_2$) in a low frequency range [18]. As a consequence, the open-loop current control system will be simplified as,

$$G_{open}(z) = z^{-1} \cdot G_{PI}(z) \cdot V_{dc} \cdot G_{notch}(z) \cdot \frac{T_s}{(z-1)(L_1+L_2)} \quad (17)$$

Subsequently, the phase margin ϕ_m of the current control system without the notch filter can be obtained as (17), where the PI controller is discretized using the Forward Euler method. Therefore, the crossover frequency ω_c can be obtained by specifying a desired phase margin.

$$\begin{aligned}\phi_m &= \pi + \angle G_{open}\left(z = e^{j\omega T_s}\right) \\ &= \pi + \angle \frac{T_s}{\left(e^{j\omega_c T_s} - 1\right)(L_1+L_2)} \cdot \frac{V_{dc}}{e^{-j\omega_c T_s}} \cdot \left(\frac{k_P T_s}{T_i\left(e^{j\omega_c T_s} - 1\right)} + k_p\right) \quad (18) \\ &= \frac{\pi}{2} - \frac{3}{2}\omega_c T_s \Rightarrow \omega_c\end{aligned}$$

In this paper, a phase margin of 60° is designed in order to guarantee enough phase margins even when the notch filter is plugged into the current control loop. This in return can ensure a phase margin around 45° for the current control system in the consideration that the notch filter introduces a phase lag around 15° at the crossover frequency ω_c. According to (18), ω_c can be obtained as,

$$\omega_c = \frac{\pi}{9T_s} \quad (19)$$

Since the crossover frequency is much smaller than the *LCL* filter resonant frequency ω_n, the gain of the notch filter is flat at the crossover frequency ω_c, and thus the notch filter has a limited impact on the crossover frequency location. Hence, (19) can be used to calculate ω_c for the entire system. Then, the rejection bandwidth Ω can be obtained by setting the phase lag of the notch filter around 15° as following:

$$\frac{\Omega T_s \cdot \omega_c T_s \cdot \cos \omega_n T_s}{2 - \Omega T_s} \cdot \frac{360}{2\pi} \approx 15^o \quad (20)$$

$$\Omega T_s \approx \frac{2\pi}{12 \cdot \omega_c T_s \cdot \cos \omega_n T_s + \pi} \quad (21)$$

As it is discussed in § IV, placing the notch frequency below the resonant frequency can contribute to an increased stability margin for the current control system. In order to achieve this goal even in a weak grid (L_g up to 10 mH [20]). The notch frequency boundary is then calculated according to (2) when L_g = 10 mH. Fig. 7 shows the Bode plot of the open-loop current control system, from which a phase margin of 43 ° can be readily identified. Fig. 8 shows the root loci in the *z*-plane of the overall current control system when the parameters of the *LCL* filter and also the grid impedance are varying. As it can be seen in Fig. 8(a), although the grid impedance L_g varies between 0 mH (a very strong grid) and 10 mH (a very weak grid), the system is always stable. However, when the grid impedance further increases ($L_g \geq$ 10 mH), the current control system goes into instability even with the notch filter based active damping. Fig. 8(b) and (c) show the stable ranges of the control system in the case of a varying inverter side inductor L_1 and grid side inductor L_2 of the LCL filter (from 50% to 150% of the value shown in Table I), respectively. It can be observed in Fig. 8(b) and (c) that for large variations of L_1 and L_2, the current control system is stable, while instability occurs when L_2 < 1.18 mH or L_1 < 1.08 mH. In Fig. 8(d), the impacts of the capacitance C_f variations (between 50% and 150% of the value shown in Table I) are analyzed. It can be seen in Fig. 8(d) that the current control system is stable in the case that C_f > 3.3 uF. However, when the capacitance decreases further, the current control system becomes unstable, as shown in Fig. 8(d). This is because that in order to tolerate a wide range of grid impedance variations (e.g., up to 10 mH), the notch frequency should be much lower than the resonant frequency. Thus, the phase lead of the notch filter will be very small at higher frequencies, as shown in Fig. 7. However, the capacitance decreases will result in an increase of the resonant frequency of the *LCL* filter, where the phase lead of the notch filter cannot prevent the open-loop system from -180°-crossing at the resonant frequency, leading to instability.

VI. Simulation and Experimental Results

Referring to Fig. 1 and Fig. 2, simulations and experiments have been performed on a 2.2-kW three-phase grid-connected inverter system in order to verify the effectiveness of the proposed notch filter based active damping. The system parameters are given in Table I. The simulations were done under ideal conditions where the inductor internal series resistances are neglected. Therefore, the simulations can also be considered as a worse case operating condition. Simulations were performed in MATLAB/Simulink. The experimental setup consists of a 2.2-kW three-phase commercial inverter connected to the grid through an *LCL* filter and an isolation transformer. The control systems are implemented in a dSPACE DS 1103 system.

Fig. 9 shows the simulation results of the proposed active damping based on a notch filter. It can be seen in Fig. 9 that the current control system can operate stable without

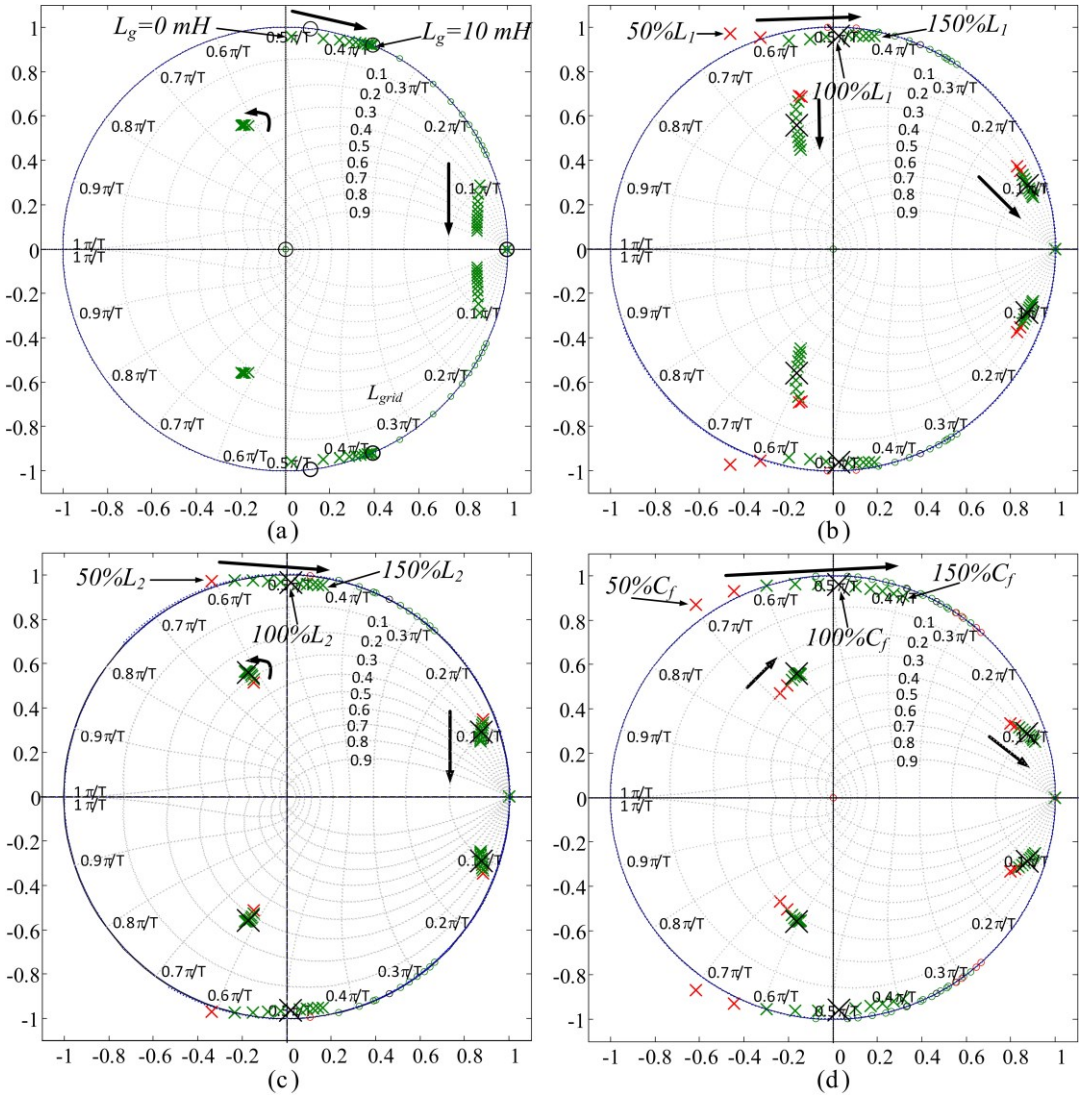

Fig. 8. Pole and zero location of the overall system when vary the grid impedance and passive elements: (a) grid impedance L_g (0 mH to 10 mH) ,(b) inverter side inductor L_1 (50% to 150%), (c) grid side inductor L_2 (50% to 150%), (d) filter capacitor C_f (50% to 150%).

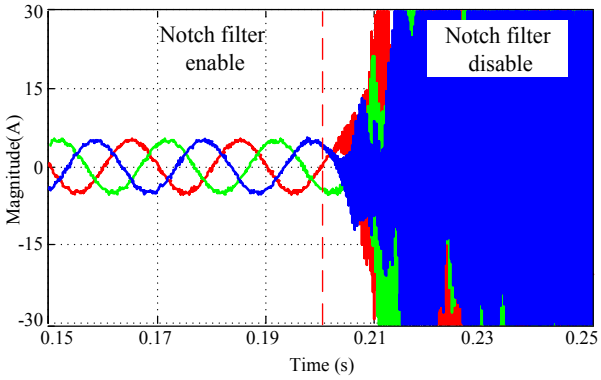

Fig. 9. Simulation results of the notch filter based active damping for a three-phase grid-connected inverter system, where the active damping is disabled at t = 0.2 s.

resonating before the active damping is disabled. This confirms that the proposed notch filter based active damping can effectively ensure the system stability – the damping is achieved by the designed notch filter.

In order to verify the effectiveness of the notch filter based active damping experimentally, the resonance of the current controller is excited by slightly increasing the proportional gain of the PI controller in the experiments. The proportional gain is then kept the same as that for a resonating system, and in that case the proposed notch filter based active damping control is enabled. Fig. 10 shows that the resonance is effectively dampened, when the proposed notch filter based active damping is activated. However, when the active damping is disabled, the resonating appears again. It is clear that an active damping is necessary for the current control system to maintain the stability and also the current quality. Those can be achieved when the proposed method is adopted, as verified by the experimental tests shown in Fig. 10. Besides, the transient performance of the proposed active damping method is also tested, where a step change of the reference grid current from 1 A to 2 A is performed according to Fig. 11. Obviously, the inverter system has good dynamic performance.

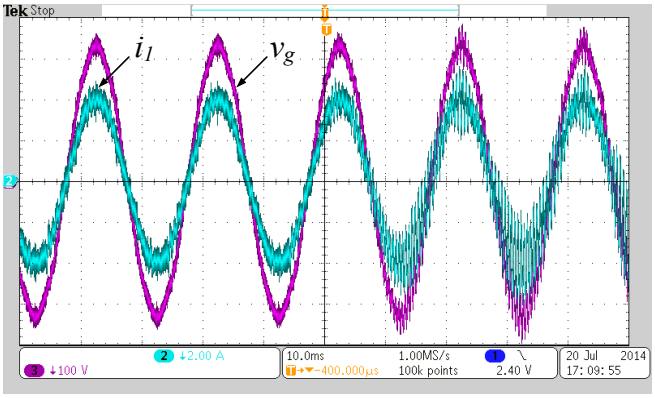

Fig. 10. Performance of notch filter based active damping: inverter phase current (Ch 1:[5A/div], and time [10ms/div]), phase voltage (Ch 2: [100 V/div], and time [10ms/div]), and enabled signal of active damping filtering.

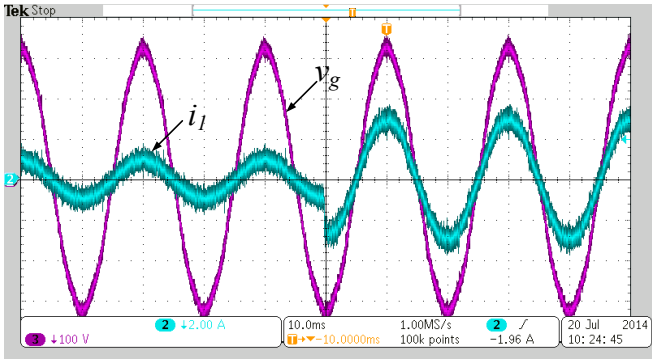

Fig. 11. Performance of notch filter based active damping: inverter phase current (Ch 1: [5A/div] and time [10ms/div]), phase volt age (Ch 2: [100 V/div] and time [10ms/div]) and enabled signal of active damping filtering.

VII. CONCLUSION

In this paper, a notch filter based active damping method has been proposed. The proposed active damping system has been analyzed and designed in the *z*-domain, and the inverter current has been fed back to the current control loop, where the proposed active damping method is incorporated. A design method of the notch filter for active damping has also been presented, and thus the phase and gain error introduced by the discretization can be minimized. The entire system stability has been investigated in the case of different resonant frequencies, which has revealed that the notch filter based active damping is sensitive to a negative variation of the resonant frequency. As a consequence, the notch filter frequency has been designed smaller than the *LCL* filter resonant frequency, which in return can ensure the system stability. A guideline for the notch filter frequency placement has been provided in this paper, enabling the use of the proposed active damping method, even when there are variations of the *LCL* filter parameter and/or the grid impedance. Both simulations and experiments have verified the effectiveness of the proposed active damping method in terms of high robustness.

REFERENCES

[1] R. Teodorescu, F. Blaabjerg, M. Liserre, and A. Dell'Aquila, "A stable three-phase LCL-filter based active rectifier without damping," in *Proc. of IEEE IAS Annu. Meeting*, pp. 1552-1557, 2003.

[2] J. Dannehl, C. Wessels, and F.W. Fuchs, "Limitations of voltage-oriented PI current control of grid-connected PWM rectifiers with LCL filters," *IEEE Trans. Ind. Electron*., vol. 56, no. 2, pp. 380-388, Feb. 2009.

[3] M. Liserre, A. Dell'Aquila, and F. Blaabjerg, "Stability improvements of an LCL-filter based three-phase active rectifier," in *Proc. of IEEE PESC'02*, pp. 1195-1201, 2002.

[4] R.Peña-Alzola, M.Liserre, F.Blaabjerg, R. Sebastián, J. Dannehl, and F. W. Fuchs, "Analysis of the passive damping losses in LCL-filter-based grid converters," *IEEE Trans. Power Electron.*, vol. 28, no. 6, pp. 2642-2646, Jun. 2013.

[5] Y. Tang, P. Loh, P. Wang, F. Choo, and F. Gao, "Exploring inherent damping characteristic of LCL-filters for three-phase grid-connected voltage source inverters," *IEEE Trans. Power Electron.*, vol. 27, no. 3, pp. 1433-1443, Mar. 2012.

[6] P. A. Dahono, "A control method to damp oscillation in the input LC-filter," in *Proc. of PESC*, vol. 4, pp. 1630-1635, 2002.

[7] V. Blasko and V. Kaura, "A novel control to actively damp resonance in input lc filter of a three-phase voltage source converter," *IEEE Trans. Ind. Appl*., vol. 33, pp. 542-550, Mar.-Apr. 1997.

[8] R. Pena-Alzola, M. Liserre, F. Blaabjerg, R. Sebastian, J. Dannehl, and F. W. Fuchs, "Systematic Design of the Lead-Lag Network Method for Active Damping in LCL-Filter Based Three Phase Converters," *IEEE Trans. Ind. Informat*., vol. 10, no.1, pp. 43- 52, Feb. 2014.

[9] Dick, S. Richter, M. Rosekeit, J. Rolink, and R. De Doncker, "Active damping of LCL resonance with minimum sensor effort by means of a digital infinite impulse response filter," *in Proc. of EPE*, pp.1-8, 2007.

[10] N. He, D. Xu, Y. Zhu, J. Zhang, G. Shen, Y. Zhang, J. Ma, and C. Liu, "Weighted average current control in a three-phase grid inverter with an LCL filter," IEEE Trans. on Power Electronics, vol. 28, no. 6, pp. 2785–2797, 2013.

[11] G. Shen, X. Zhu, J. Zhang, and D. Xu, "A new feedback method for PR current control of LCL-filter-based grid-connected inverter," *IEEE Trans. Ind. Electron*., vol. 57, no. 6, pp. 2033-2041, Jun. 2010.

[12] W. Gullvik, L. Norum, and R. Nilsen, "Active damping of resonance oscillations in LCL-filters based on virtual flux and virtual resistor," *in Proc. of EPE.* pp. 1-10, 2007.

[13] J. Dannehl, M. Liserre, and F. Fuchs, "Filter-based active damping of voltage source converters with LCL-filter," *IEEE Trans. Ind. Electron.*, vol. 58, no. 8, pp. 3623-3633, Aug. 2011.

[14] M. Liserre, A. Dell'Aquilla, and F. Blaabjerg, "Genetic algorithm based design of the active damping for a LCL-filter three-phase active rectifier," *IEEE Trans. Power Electron*., vol. 19, no. 1, pp. 234-240, Jan. 2003.

[15] C. Xie, Y. Wang, X. Zhong, and C. Chen, "A novel active damping method for LCL-filter-based shunt active power filter," *in Proc.of IEEE ISIE'12,* 2012, pp. 64–69.

[16] K. Hirano, S. Nishimura, S.K. Mitra, "Design of Digital Notch filter," *IEEE Trans. Circuits and Systems*., vol. 21, no. 4, pp. 540-546, Jul. 1974.

[17] P.A. Regalia, S.K. Mitra, P.P. Vaidyanathan, "The Digital All-Pass Filter: A Versatile Signal Processing Building Block," *Proc. of IEEE*., vol. 76, no. 1, pp. 19-37, Jan. 1988.

[18] S. Parker, B. P. McGrath, and D. G. Holmes, "Region of active damping control for LCL filters," *IEEE Trans. Ind. Appl*., vol. 50, no. 1, pp. 424-432, Jan.-Feb. 2014.

[19] A. G. Yepes, F. D. Freijedo, J. Doval-Gandoy, O. Lopez, J. Malvar, and P. Fernandez-Comesana, "Effects of discretization methods on the performance of resonant controllers," *IEEE Trans. Power Electron*., vol. 25, no. 7, pp. 1692-1712, Jul. 2010.

[20] M. Liserre, R. Teodorescu, and F. Blaabjerg, "Stability of photovoltaic and wind turbine grid-connected inverters for a large set of grid impedance values," *IEEE Trans. Power Electron.*, vol. 21, no. 1, pp. 263-272, Jan. 2006.